Ceramics International 44 (2018) 6801–6809

Contents lists available at ScienceDirect

Ceramics International

journal homepage: www.elsevier.com/locate/ceramint

Hollow spherical and nanosheet-base BN nanoparticles as perspective additives to oil lubricants: Correlation between large-scale friction behavior and *in situ* TEM compression testing

A.V. Bondarev[a], A.M. Kovalskii[a], K.L. Firestein[a,b], P.A. Loginov[a], D.A. Sidorenko[a], N.V. Shvindina[a], I.V. Sukhorukova[a], D.V. Shtansky[a,*]

[a] National University of Science and Technology "MISIS", Leninsky prospect 4, Moscow, Russia
[b] School of Chemistry, Physics and Mechanical Engineering, Queensland University of Technology (QUT), 2nd George st., Brisbane QLD 4000, Australia

ARTICLE INFO

Keywords:
A. Powders: gas phase reaction
C. Friction
C. Mechanical properties
D. Nitrides

ABSTRACT

In the present study we utilized *h*-BN nanoparticles (NPs) with different morphologies (hollow NPs with smooth surface (H-BNNPs), solid NPs with "pompon"-like or petalled structure (P-BNNPs), and globular NPs formed by numerous thin *h*-BN nanosheets (N-BNNPs)) as additives to PAO6 oil. Two sliding 100Cr6 surfaces were tested in the presence of PAO6 + BNNP lubricants with 0.1% and 0.01% of BNNPs. The positive effect of BNNP additives increased along the row P-BNNPs → H-BNNPs → N-BNNPs. Utilization of N-BNNPs permitted to decrease noticeably the friction coefficient from 0.1 to 0.06 and reduce significantly the wear rate. In situ mechanical TEM tests were also performed to visualize and correlate the mechanical properties of individual *h*-BN NPs to their large-scale friction behavior.

1. Introduction

Although the lubricant market is developing rapidly, control over friction and wear is still a challenge that influences a broad range of material applications from machine and engine components to electromechanical systems, material processing, and medical devices. Friction and wear are known to result in huge energy and financial losses. The problem of global energy consumption due to friction was recently reviewed by Holmerg et al. [1–3] In order to increase reliability and durability of the friction assemblers and enhance energy efficiency of tribomechanical systems, different types of both dry and liquid lubricants are widely used worldwide. Depending on the type of lubricant, reduced friction and wear between two sliding surfaces are achieved by forming either a continuous and stable fluid film or self-lubricating solid tribofilm. Currently, liquid lubricants with various additives to impart desired characteristics dominate the market. There are numerous studies showing that the lubricant characteristics can be improved by adding micro- or nanoparticles [4–17]. The friction reduction and anti-wear mechanisms were reported to be dependent on size, shape, and concentration of particles, as well as on their mechanical strength and chemical stability. A complete review of recent developments in the field of friction modifiers for liquid lubricants was compiled by Tang and Li [18] and recently supplemented by Dai *et al.* [19] Nanoparticles (NPs), as lubricant additives, can be divided into several types: carbon and its derivatives, soft metals, metal oxides based on Magneli phases, transition metal dichalcogenides (TMDs), rare earth compounds, nanocomposites, and others, for instance $CaCO_3$, polytetrafluoroethylene, and BN. While well-known solid lubricants owe lubricity to their layered structure, solid NPs can provide additional lubrication mechanisms such as (a) rolling, (b) sliding, and (c) exfoliation [20–23]. It has been found that rolling of NPs occurs at low shear rates and pressures, which depends on the spherical shape of the particles and their mechanical stability. The sliding of NPs is also dependent on the mechanical strength and the amount of interfacial adhesion. In case of exfoliation, the outer layers of NPs delaminate under higher shear stress and pressures. The generated nanosheets are transferred to the contact region and align in the direction of sliding, thereby reducing friction through formation of a tribofilm. In addition, NPs themselves can participate in the formation of protective tribolayer with a specific orientation and its low shear basic planes parallel to the sliding direction [24–26]. Adding soft-metal NPs can also lead to an excellent mending effect [27].

NPs can be obtained in different size and morphology, for instance hollow and solid cores, smooth and petalled surfaces, which is believed to influence greatly their tribological performance. However, little work has been done so far to explore and take advantage of each

* Correspondence to: National University of Science and Technology "MISIS", 4 Leninsky Ave., Moscow 119049, Russia.
E-mail address: shtansky@shs.misis.ru (D.V. Shtansky).

https://doi.org/10.1016/j.ceramint.2018.01.101
Received 28 November 2017; Received in revised form 28 December 2017; Accepted 13 January 2018
Available online 31 January 2018
0272-8842/

morphology in a specific application. Although the available data are rather incomplete and contradictive, there is clear evidence that the best tribological characteristics are achieved with a certain shape and size of NPs [28–33].

Hexagonal boron nitride (*h*-BN) is a layered and environmentally friendly material with high potential as an additive to oil lubricants due to a combination of excellent lubricating properties and superb resistance to oxidation, profound chemical inertness, high thermal stability and thermal conductivity, as well as good biocompatibility [34]. Spherical BN NPs (BNNPs) of various morphologies (solid "onion"-like particles with smooth surfaces, solid "pompon"-like particles, hollow thin- and thick-shelled particles with either smooth or petalled surfaces) were recently fabricated through high-temperature boron oxide-assisted CVD technique (BOCVD) [35].

The use of *h*-BNNPs as additives to liquid lubricants was reported in a number of studies. For instance, *h*-BN nano-sheets were proposed to be a promising "green" lubricant additive for water [36]. Their enhanced tribological properties were attributed to tribo-films formed on the worn surface by repeated exfoliation and deposition of *h*-BNNPs [36,37]. Even relatively small amount of *h*-BN additives (1.0 wt%) was shown to significantly reduce friction and wear of Si_3N_4/DLC films in PAO6 base oil [38]. The observed superlubricity was explained by a decrease in the contact area due to the presence of *h*-BN nanoparticles acting as ball bearings. Hexagonal BN was also utilized with high thermal conductivity dielectric oils designated for thermal management [39].

To achieve the maximum effect from BN additives, the choice of their optimal concentration is very important. High BNNP concentration causes a deterioration of lubrication due to particle agglomeration, while reduced wear can be achieved even at BN concentration as low as < 0.1% [40–44]. As additives to liquid lubricants, *h*-BN particles are of special interest due to their highly disordered microstructure often described as turbostratic [45]. Poorly crystalline particles usually generate a more homogeneous tribofilm and often demonstrate lower friction coefficient as they have more defects and are prone to easier exfoliation. Thus in the present study for the first time we utilized *h*-BNNPs obtained *via* BOCVD method with three different morphologies as additives to PAO6 oil: (i) hollow particles with smooth surface, hereinafter referred to as H-BNNPs, (ii) solid particles with "pompon"-like or petalled structure, hereinafter abbreviated as P-BNNPs, and (iii) globular particles formed by numerous thin *h*-BN nanosheets, designated as N-BNNPs. Friction and wear, as two interactive responses from a tribo-system mutually affecting each other, were thoroughly studied. *In situ* mechanical TEM tests were also performed to visualize and correlate the mechanical properties of individual NPs to their large-scale friction behavior.

2. Materials and methods

2.1. Synthesis of BN nanoparticles

BNNPs were synthesized *via* a BOCVD process in a vertical inductively-heated reactor as described elsewhere [35]. Two types of powder mixtures were used as precursors: (i) amorphous B (99.9%), MgO (analytical grade), and pure FeO taken in a molar ratio of 3.5:0.1:1 (H-BNNPs) and 3.5:0.4:1 (N-BNNPs), and (ii) $BLiO_2$ (99.9%) (P-BNNPs). Magnesia was calcined in air at 450 °C for 1 h for dehydration just before weighing. Precursor mixtures were mechanically ground in a mechanical alumina mortar for 1 h with addition of isopropanol. Argon of 99.993% purity was used as a carrying gas, supplied with the feed rate of 300–500 cm^3/min from the bottom of the reactor, and ammonia of 99.98% purity was used as the reactant gas, supplied with the feed rate of 50–100 cm^3/min from the top. Thus the Ar/NH_3 flow ratio was maintained from 3 to 6 to promote the nucleation and growth of specific BNNP morphology: P-BNNPs (Ar/NH_3 = 3), H-BNNPs (Ar/NH_3 = 5), and N-BNNPs (Ar/NH_3 = 6). At first, the furnace chamber was evacuated to 10^{-2} mbar under slow heating to 360 °C. Then, an argon flow was introduced, the total pressure of 1 bar was maintained, after which the system was heated to a required temperature depending on the type of NPs. Syntheses were carried out under a temperature gradient along the reactor height with higher temperatures in the precursor zone and lower temperatures (700–750 °C) in the BNNP outlet zone. The synthesis temperature in the precursor zone was 1310 (H-BNNPs) and 1400 °C (P-BNNPs and N-BNNPs). The temperature of the powder mixture was controlled by optical pyrometer during the whole experiment.

2.2. Structural characterization

The microstructure of as-synthesized BNNPs and wear debris after tribological tests were studied using a JEM7700F scanning electron microscope (JEOL) and a JEM-2100 transmission electron microscope (JEOL) equipped with an energy dispersive spectroscopy (EDS) system (Oxford Instruments). The chemical composition of BNNPs was analyzed using a Vertex 70 v vacuum IR spectrometer (Bruker). The wear tracks after tribological tests were examined by a scanning electron microscope S-4800 (Hitachi) equipped with an X-ray microanalyzer NORAN System 7 (Thermo Scientific).

2.3. Tribological tests

To prepare lubricating suspensions, each type of BNNPs in the amount of 0.01% and 0.1% was added into 30 ml of PAO6 oil (Neste) and then twice sonicated for 10 min with an interval of 5 min. A pin-on-plate tribometer (CSM Instruments) was employed to study the tribological characteristics of a 100Cr6 friction pair in the presence of PAO6 + BNNPs lubricants. The average surface roughness R_a of the 100Cr6 plates used in trobological tests was 5 ± 1 nm. The tests were performed at room temperature in multipass reciprocating mode using a 3 mm-sized 100Cr6 ball as counterpart material. The normal load and sliding speed were 1 N and 0.05 m/s, respectively. Under these conditions each sample passed 10,000 cycles. The wear track profiles were measured using a WYKO NT1100 optical profilometer (Veeco).

2.4. In situ mechanical tests of BN nanoparticles

In situ TEM compression testing of individual BNNPs was performed using a JEM 2100 microscope (JEOL) equipped with a depth-sensing PI 95 TEM Picoindenter (Hysitron). The BNNP deformation was observed and recorded in real time using Radius and Hysitron TriboScan software applications (Olympus and Hysitron respectively). During deformation, force-time and force-displacement curves were recorded. The compression tests were carried out using a diamond flat-end conical tip with 1 μm diameter of the top circle. Samples were loaded at a rate of 24 nm/s and then exposed at maximal displacement of 120 nm for 5 s.

3. Results and discussion

3.1. Microstructure of as-synthesized BNNPs

SEM images of all three types of BNNPs are presented in Fig. 1. Structural investigations exhibited that the as-prepared white-colored powder (Fig. 1e) consisted of BNNPs with different shapes, the latter being dependent on fabrication conditions. The surface of P-BNNPs having a diameter of 50–300 nm is formed by numerous *h*-BN nanosheet-like petals (Fig. 1a). The N-BNNPs with sizes of 300–700 nm are BN nanosheet agglomerates with a length of an individual nanosheet reaching 200–300 nm (Fig. 1b). The H-BNNPs, 50 – 300 nm in diameter, have a hollow core and a smooth surface (Fig. 1c).

The FTIR spectra of the as-synthesized BNNPs are shown in Fig. 1d. All types of BNNPs are characterized by two main common maxima at ~1350 and ~770 cm^{-1} assigned to in-plane and out-of-plane BN

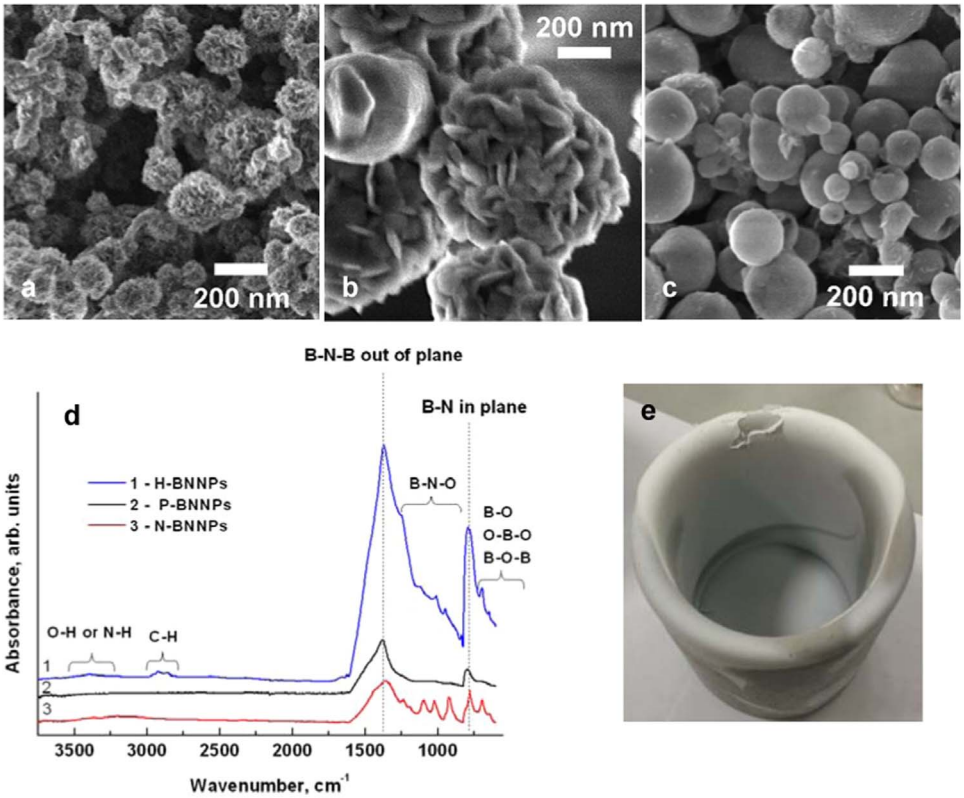

Fig. 1. (a)-(c) SEM images of different types of BNNPs and (d) their FTIR spectra. (e) Crucible with product prepared in this study (seen as white powder).

stretching vibrations, respectively. The P-BNNPs was the only sample that exhibited FTIR spectrum similar to that of pure bulk *h*-BN. The FTIR spectra of the H-BNNPs and the N-BNNPs demonstrated two broad bands at 850 – 1260 and 600 – 720 cm^{-1}, with high absorbance indicating various bonds of B and N with oxygen: B-O, O-B-O, B-O-B and B-N-O. Additional small features observed in the FTIR spectrum of the H-BNNPs in the ranges of 2700 – 2900 and 3000 – 3500 cm^{-1} can be ascribed to O-H and C-H bonds.

Fig. 2 shows TEM images of the BNNPs at both low (top row) and high (low row) magnifications. Detailed TEM analysis revealed the microstructural features of all three types of BNNPs. The outer surface of the P-BNNPs is seen to be formed by numerous curved BN petals 10–20 nm in length and 5–10 nm in width, with a characteristic interplanar spacing of 0.33 nm (Fig. 2a,d). The inner part of the P-BNNPs consisted of small highly disordered regions, several nm in thickness. This type of structure is often described as a turbostratic BN [45]. The N-BNNPs are seen to be formed by numerous elongated BN nanosheets up to 100 nm in length. The BN nanosheets are randomly oriented in space and agglomerated in spheroidal particles (Fig. 2b). Their hexagonal BN layers are observed to be free of defects and have a characteristic interplanar spacing of 0.33 nm (Fig. 2e). The H-BNNPs with an average size of 50–200 nm revealed nearly spherical morphology

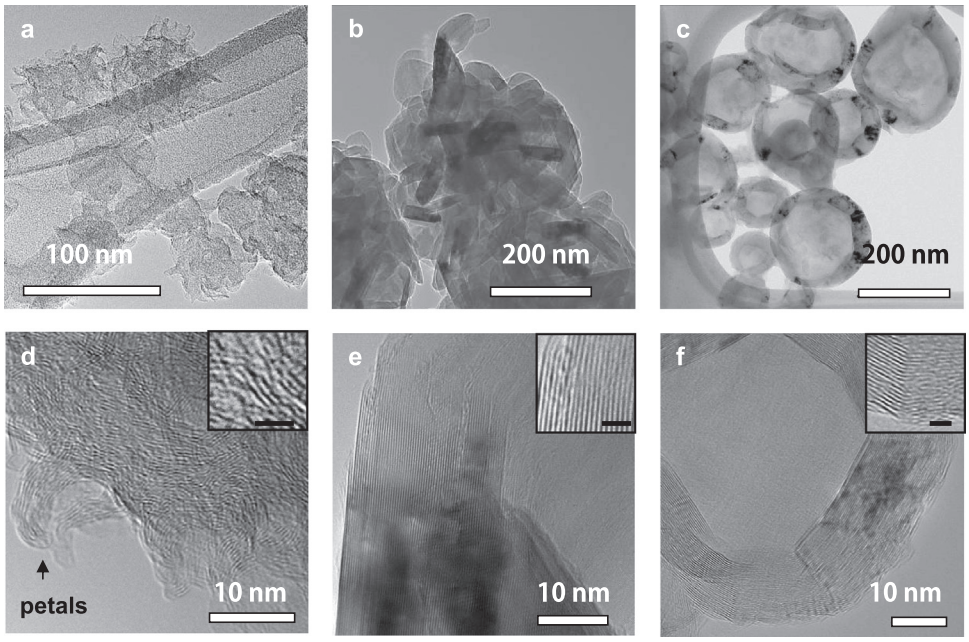

Fig. 2. (a-c) TEM and (d-f) high-resolution TEM images of BNNPs with different morphologies. Scale bars in inserts (d)-(f) correspond to 2 nm.

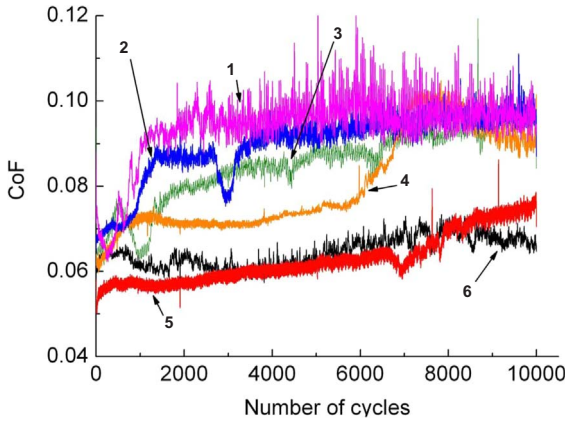

Fig. 3. Coefficient of friction recorded during sliding of two 100Cr6 surfaces (pin-on-plate configuration in multipass reciprocating mode) in the presence of different suspensions: 1 - PAO6, 2 - PAO6 + 0.01P-BNNPs, 3 - PAO6 + 0.1P-BNNPs, 4 - PAO6 + 0.1H-BNNPs, 5 - PAO6 + 0.01N-BNNPs, 6 - PAO6 + 0.1N-BNNPs.

with a hollow central part and shells with a thickness of about 25–50 nm (Fig. 2c). The shell thickness of an individual NP can also vary. Every shell consisted of numerous subgrains with hexagonal planes oriented approximately parallel to the surface (Fig. 2f). Note that misfit dislocations were frequently observed at the subgrain boundary interfaces.

3.2. Tribological tests

Fig. 3 shows the results of tribological tests of a 100Cr6 ball on a 100Cr6 plate in the presence of PAO6 + BNNPs lubricants performed at room temperature in reciprocal mode. It is clearly seen that the use of pure PAO6 oil (as reference) led to significant fluctuations of friction coefficient (CoF) and their value fell within the range of 0.09 – 0.10, being the highest among all samples tested (Fig. 3, curve 1). The use of PAO6 + P-BNBNs with the concentration of BNNPs 0.01% led to a slight decrease in CoF, but only at the beginning of the test (Fig. 3, curve 2). When the concentration of P-BNNPs in PAO6 was increased to 0.1%, the CoF further decreased but still remained relatively high (Fig. 3, curve 3). When using PAO6 oil with H-BNNP additives, the results of tribological tests were similar regardless of the amount of BNNPs, which is why only one friction curve for the PAO6 + 0.1H-BNBN lubricant was plotted in Fig. 3. Note that addition of H-BNNPs permitted to keep CoF value close to 0.07 for as many as 6000 cycles, after which the sample with 0.1% of H-BNNPs (Fig. 3, curve 4) demonstrated CoF values similar to those of samples with pure PAO6 (curve 1) and PAO6 + P-BNNPs (curves 2 and 3). In case of PAO6 + N-BNBN suspensions, the CoF values were observed to be the lowest, only slightly increasing from 0.06 to 0.07 by the end of the tests (Fig. 3, curves 5 and 6).

Fig. 4 compares optical images, 3D images and 2D wear track profiles of 100Cr6 surfaces after tribological tests with pure PAO6 and PAO6 + BNNPs suspensions with different types of BNNPs and concentrations. In addition, the wear rates of counterpart material are also shown below each 2D optical image. Before these observations, all the samples were gently sonicated in isopropanol for 5 min; thus it is reasonable to assume that most of wear debris remained inside the wear tracks. Without BNNP additives, the ball wear rate was equal to 2.50×10^{-7} mm^3/Nm and the surface of counterpart material in the area of tribological contact was free from wear debris (Fig. 4a). The middle area of the wear track exhibited a positive wear with the maximum height (h_m) of the wear products stuck at the bottom of wear track equal to $h_m = 0.15$ μm, whereas both abrasive and adhesive wear modes were observed at the wear track edges(Fig. 4a).

When tribological tests were performed using PAO6 + 0.01P-BNNP suspension, the wear rate of counterpart material slightly decreased to 9.0×10^{-8} mm^3/Nm (Fig. 4b). No adhered wear debris were observed on the surface of counterpart material. Analysis of the 2D wear track profiles indicates the formation of a thin tribolayer in the middle of the track (h_m = 0.05 μm) and abrasive wear at the edges (the maximum (d_m) and average (d_a) wear track depths were 0.12 and 0.04 μm, respectively). With increasing P-BNNP concentration to 0.1 wt%, the wear rate of 100Cr6 ball significantly increased to 1.88×10^{-5} mm^3/Nm (Fig. 4c). The wear process was accompanied by intensive formation of wear products on both surfaces of friction pair (h_m = 0.25 μm). Since the CoF values were similar for both BNNP suspensions (with 0.1% and 0.01% of BNNPs), we can assume that the wear products did not affect friction. Therefore, only a small amount of P-BNNP additives (0.01 wt%) led to a slight improvement in tribological characteristics.

When adding 0.01 wt% of H-BNNPs to PAO6, the value of wear rate of 100Cr6 ball was 1.40×10^{-7} mm^3/Nm, *i.e.* similar to pure oil (Fig. 4d). The 100Cr6 ball wear rate was observed to decrease to 7.20×10^{-8} mm^3/Nm when the H-BNNP concentration was raised to 0.1 wt % (Fig. 4e). Note that the surface of counterpart materials was mainly free from wear debris. In case of 0.1 wt% of H-BNNPs, the maximum thickness of tribolayer in the middle part of wear track was significantly smaller than at low H-BNNP concentration (h_m = 0.04 μm *versus* h_m = 0.08 μm). Both samples showed abrasive wear on the wear track edges, but the wear products were observed to accumulate more intensively at the bottom of wear track when adding 0.01 wt% of H-BNNPs. To sum up, addition of 0.1 wt% of H-BNNPs to PAO6 oil permitted to reduce both CoF (from 0.1 to 0.07) and wear rate (from 2.5×10^{-7} to 7.2×10^{-8} mm^3/Nm).

The best tribological characteristics were obtained using PAO6 + 0.01N-BNNP suspension (Fig. 4f,g). Addition of N-BNNPs into PAO6 led to a noticeable decrease in CoF from 0.1 to 0.06 and a significant decrease in the ball wear rate to 1.34×10^{-8} (0.01 wt% of N-BNNPs) and 1.08×10^{-9} mm^3/Nm (0.1 wt% of N-BNNPs). The size of tribological contact zone on the surface of counterpart material was the smallest among all the samples tested. Importantly, wear track on the surface of 100Cr6 plate was hardly detected. The 2D wear track profiles were relatively flat indicating no abrasive wear and no formation of wear products (Fig. 4g).

Fig. 5 summarizes the effect of the type and concentration of BNNPs in PAO6 + BNNP suspension on the wear rate of counterpart 100Cr6 material. All oil lubricants with 0.01 wt% of BN additives showed a decrease of the ball wear rate, wherein the maximum effect was observed for the N-BNNPs. With increase in BNNP concentration, the counterpart materials demonstrated different wear behavior depending on particle morphology: further decrease of wear rate for the H-BNNPs and N-BNNPs while a sharp increase of wear rate for P-BNNPs.

3.3. Structural characterization of wear products

Samples tested using pure PAO6 oil (control) and PAO6 + 0.1N-BNNP suspension that showed the best tribological characteristics were selected for more detailed SEM and EDS analysis (Fig. 6). Of all samples tested, the thickness of wear track was the maximum for the sample treated with pure PAO6 oil (350 μm). In case of the PAO6 + 0.1N-BNNP suspension, the wear track borders were not visible. In backscattered electrons (BSE) TOPO contrast, the SEM images of the selected areas of wear track observed after the tribological test in pure PAO6 oil show a characteristic corroded surface due to abrasive wear (Fig. 6a). In addition, small scratches parallel to the sliding direction are well seen in Fig. 6a. The surface of counterpart material was also badly worn and the wear debris mainly in the form of iron and chromium oxide segregated on the edges of the tribocontact area (Fig. 6d). Oxygen EDS mapping (Fig. 6b) and oxygen compositional cross-track profile (Fig. 6c) revealed a large amount of oxidized wear products inside the wear track. Thus the surface damage was caused by fretting wear as a result of simultaneous exposure to abrasion and corrosion.

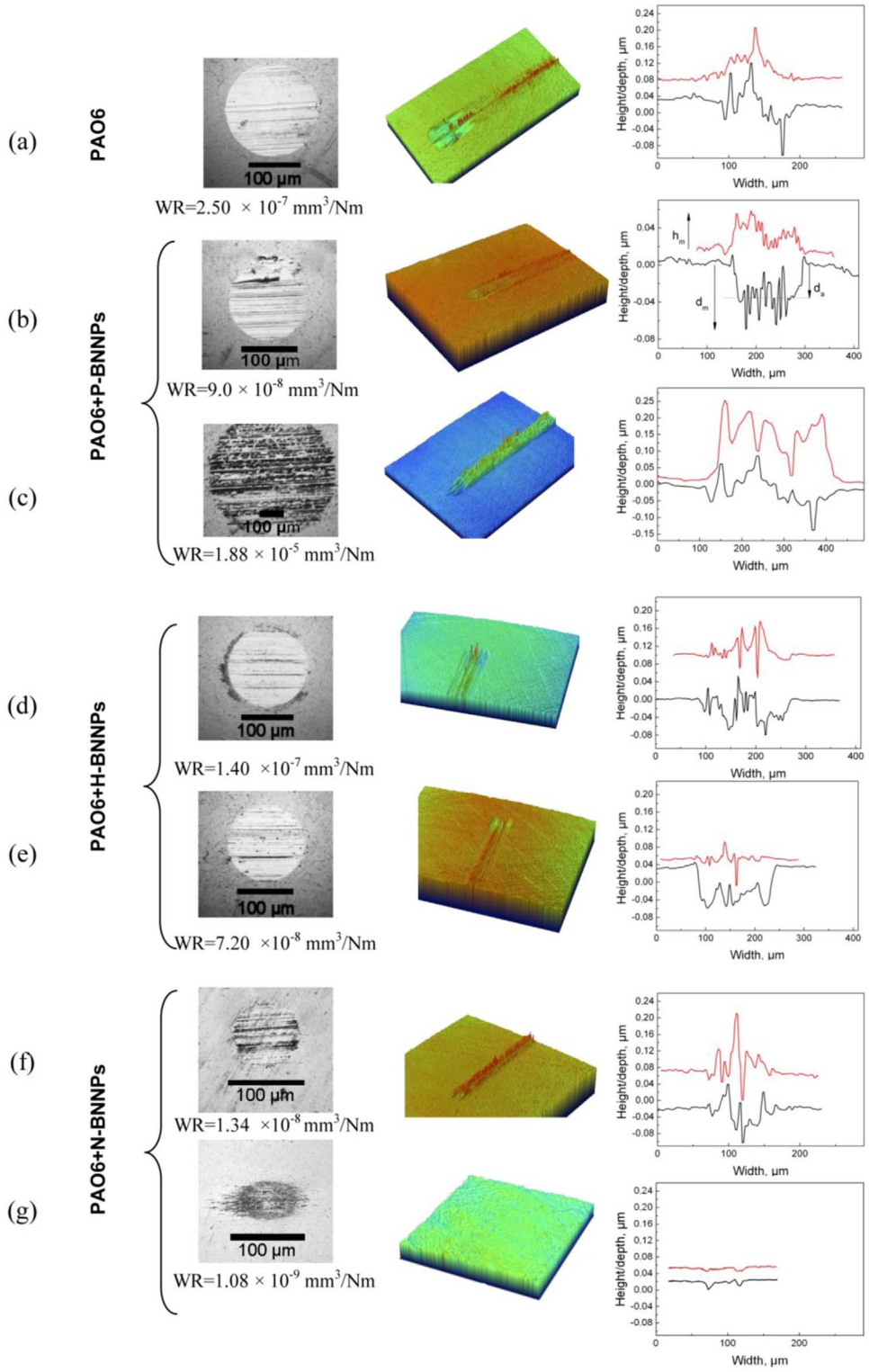

Fig. 4. Optical images (left), 3D surface images (middle), and 2D wear track profiles (right) obtained in the middle (top) and at the end of the track (bottom). All data were recorded after reciprocal 100Cr6 ball on 100Cr6 plate tribological tests in the presence of different types of PAO6 + BNNPs lubricants with 0.01 wt% of BNNPs (top) and 0.1 wt% of BNNPs (bottom). W*R* indicates the average value of ball wear rate.

After the tests using PAO6 + 0.1N-BNNP suspension, the wear track was hardly detected using SEM. The wear of counterpart material was also low, typically below 10^{-9} mm^3/Nm. The surface of as-tested samples revealed oil residues in the zone of tribological contact containing N-BNNP agglomerates aligned along the sliding direction (Fig. 6e, left SEM image). After sonication, which led to the removal of oil residues, the wear track bottom was covered with numerous N-BNNP agglomerates, 200–800 nm in size (Fig. 6e, right SEM images). Since no scratches or eroded zones were observed in the sliding direction, it is reasonably to assume no wear of the 100Cr6 plate. This result indicated that the N-BNNP agglomerates did not form a continuous tribolayer, but completely isolated two surfaces from each other during sliding. It should be remarked that such a significant positive effect of adding N-BNNP was achieved at rather low BNNP content, 0.1 at%. Note that the formation of tribolayer when using NP-doped suspensions was typically observed at higher NP concentrations about 0.5 – 5 wt% [46–49].

In order to uncover the role of BNNP morphology in the tribological

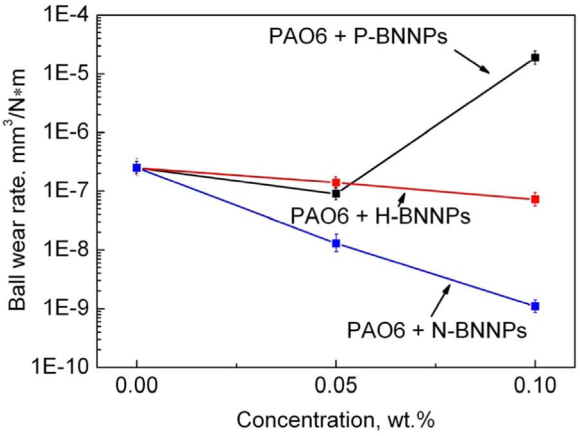

Fig. 5. Effect of the type and concentration of BNNPs in PAO6 + BNNP suspension on the wear rate of counterpart material.

performance of 100Cr6 friction pair, after the tests the BNNPs were characterized by TEM. Since it is difficult to remove oil prior to TEM analysis, additional model tribological tests were carried out using isopropanol with 0.1 wt% of BNNP additives. Before applying lubricants, the suspensions were sonicated using the same regimes as the PAO6 + BNNPs. After the tests, the wear debris were collected from the 100Cr6 ball surface and placed onto a carbon TEM grid. Thorough structural analysis of the wear debris on the grid surface revealed two types of wear products: (i) agglomerates of BN nanoplates and (ii) 100Cr6 debris (Fig. 7a). The size of agglomerates (about 300 nm) was much smaller compared with the initial N-BNNPs and the agglomerates were formed by only several BN nanosheets stuck together. This result indicates that under applied load, the initial N-BNNPs disintegrated with the formation of individual BN nanosheets. The nanosheets could be easily aligned with their basal hexagonal planes parallel to sliding direction hereby minimizing wear and providing good lubrication. The 100Cr6 debris were observed to be small, typically 5 – 15 nm (Fig. 7a), and also form agglomerates.

Three types of wear products were observed after the tribological tests using suspension with H-BNNPs: initial "pompon"-like NPs, BNNPs without inner petals, and steel debris (Fig. 7b). The results indicate that the number of small petals detached from BN core was not high enough to contribute significantly to the friction reduction, whereas the shapeless form of BNNPs apparently was not optimal to minimize friction and wear. The hollow BNNPs retained their spherical morphology after the tribological tests (Fig. 7c). Thus they were able to withstand high applied loads and appeared to provide lubrication due to rolling effect.

Summarizing the results of model tribological tests, the following conclusions can be drawn. (i) P-BNNPs had irregular shape and did not form any oriented structures to minimize the resistance to shear. Their numerous small BN petals partially detached during the tests and could align parallel to sliding direction hereby reducing friction. However, their amount was not enough to make any noticeable contribution to

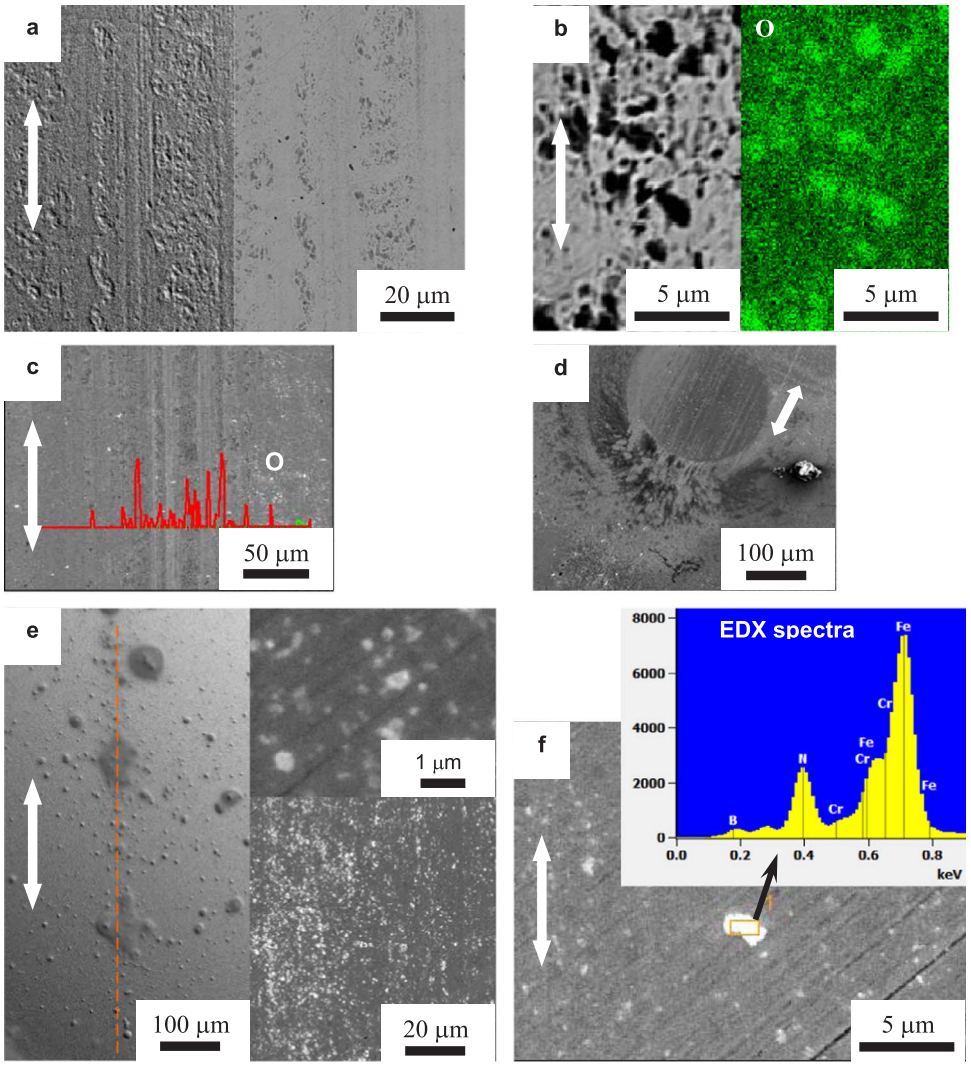

Fig. 6. SEM images, oxygen EDS mapping (right part of the image in panel (b)), and EDS spectrum (panel (f), insert) of the selected wear tracks and (d) counterpart material areas obtained after tribological tests using (a-d) pure PAO6 oil and (e, f) PAO6 + 0.1%N-BNNPs suspensions. (a) BSE TOPO (left) and COMPO (right), (b) BSE COMPO, (c,d) SE, (e) BSE TOPO (left) and SE (right), (f) SE. Left part of panel (e) shows the SEM image of wear track until oil suspension was removed. Arrows show sliding directions.

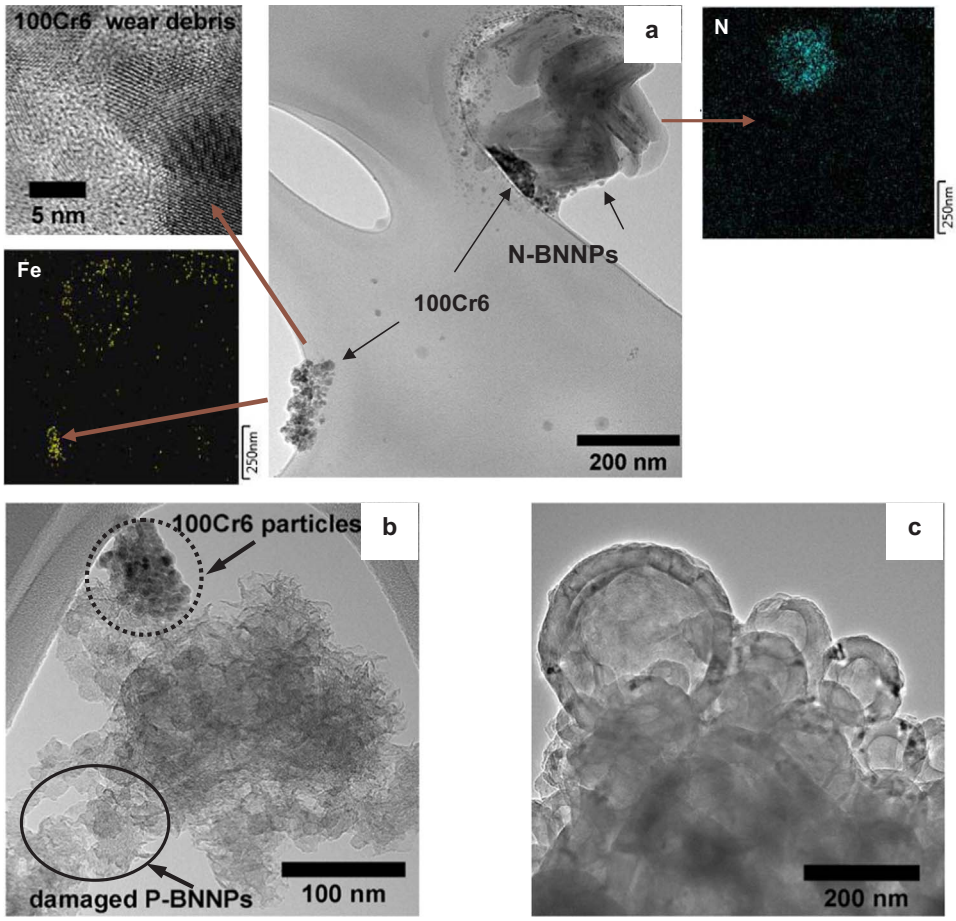

Fig. 7. TEM images of (a) N-BNNPs (with corresponding EDS mapping and high resolution TEM image), (b) P-BNNPs, and (c) P-BNNPs after model tribological tests.

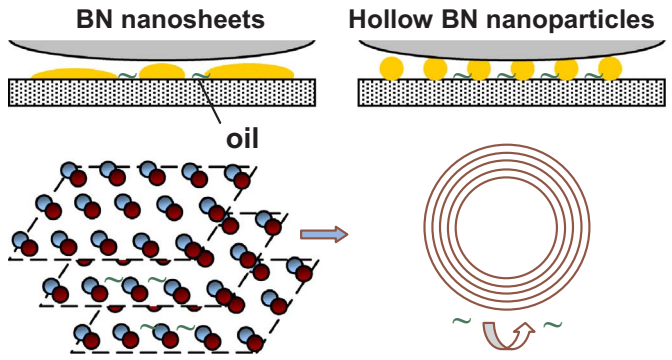

Fig. 8. Schematics of possible wear mechanisms using PAO6 + BNNP lubricants with BN nanosheet-based (left) and hollow spherical BN nanobearings.

improve tribological characteristics. (ii) Since the H-BNNPs retained their shape and morphology, their main contribution to the friction and wear reduction could be due to rolling mechanism of lubrication (Fig. 8). (iii) The N-BNNPs partly disintegrated to individual nanosheets and could easily reorient themselves normal to the applied load and contribute significantly to friction and wear reduction. In addition, BN nanosheets formed agglomerates uniformly distributed over the area of tribological contact, thereby almost completely isolating two rubbing surfaces. Within oiled agglomerates, such BN nanosheets can easily move with respect to each other due to weak Van der Waals forces and thus can be considered as smart flat nanobearings (Fig. 8). Finally note that small BN particles acting as nanoabrasive caused only nanometer-size steel wear debris, which is expected to prevent intensive wear and contribute to the efficient and long-term performance of tribomechanical systems.

3.4. *In situ* mechanical testing of BNNPs

In order to shed light on the mechanical behavior of BNNPs under applied loads, *in situ* compression tests were conducted in the TEM column to uncover directly the BNNP deformation mechanisms. The N-BNNPs were observed to disintegrate easily into separate BN nanosteets when indenter tip touched the sample surface (not shown). Fig. 9a,b displays the images of a single BN nanosheet in which the wide face was parallel to applied load both before and after deformation. During deformation, the contact area between the BN nanosheet and counterpart material became flat with a great degree of alignments of the basal hexagonal planes parallel to the friction direction (Fig. 9b(inset)). This minimizes the resistance to shear during friction.

The H-BNNPs were tested in the process of multicyclic loading. A set of images extracted from a video recording during compressive test of a single H-BNNP under maximum applied load of 3.5, 5.2, 5.9, 6.9, and 7.8 μN during each loop (Fig. 9i) is shown in Fig. 9c-h. The tested H-BNNP had the outer diameter of 165 and shell thickness varying from 15 to 40 nm. At low applied loads, typically below 6 μN, the H-BNNP was observed to retain its size and spherical shape (Fig. 9d). After the fifth loading-unloading loop with the maximum load of 7.8 μN, which led to maximal compression about 25% of the original sphere diameter (Fig. 9g), the contact zone became flat, indicating 10% of plastic deformation (Fig. 9h). During multicyclic loading (5 cycles) the BNNP withstood an applied load of 7.8 μN without failure, wherein the maximum contact area (calculated assuming that BNNP retained its spherical shape as shown in Fig. 9g) was 5.2×10^3 nm^2 and the maximum contact pressure reached 1.5 GPa. This value is an order of magnitude larger than the contact pressure of 0.13 GPa estimated from the size of tribological contact zone (100 μm) measured after the tribological test using the PAO6 + H-BNNPs suspension at an applied load

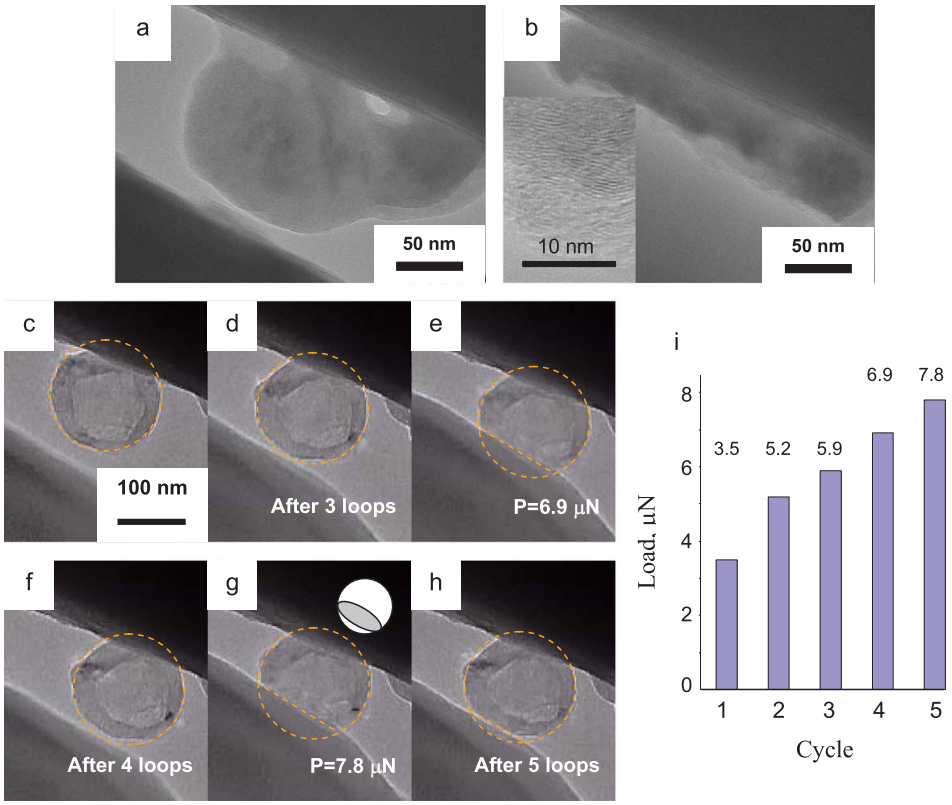

Fig. 9. Extracted video images of *in situ* compression test. (a, b) Individual BN nanosheet from N-BNNP (a) before and (b) after deformation at a maximum load of 120 μN. (c-h) Screenshots from the video showing H-BNNP deformation during five load-unload loops under gradually increased load as shown in panel (i).

of 1 N. Thus, the main lubrication mechanism for the H-BNNPs could be rolling similar to that observed for fullerene-like MoS_2 particles [50]. Finally note that the H-BNNPs may also play a role of spacers between contacting surfaces, hereby preventing adhesion and sticking of their materials. All these factors may favorably affect the role of BNNPs as solid additives to lubricants.

4. Conclusions

In the present study we utilized hexagonal BN nanoparticles (BNNPs) with different morphologies (hollow particles with smooth surface (H-BNNPs), solid particles with “pompon”-like or petalled structure (P-BNNPs), and globular particles formed by numerous thin *h*-BN nanosheets (N-BNNPs)) obtained *via* boron oxide-assisted chemical vapor deposition method as additives in an amount of 0.01 and 0.1 wt% to PAO6 oil. The obtained results were summarized as follows.

1. The positive effect of BNNP additives increases along the row P-BNNPs → H-BNNPs → N-BNNPs. The best tribological characteristics of 100Cr6 friction surfaces were achieved by using PAO6 + 0.1N-BNNP lubricants: the friction coefficient and wear rate decreased from 0.1 to 0.06 and from 2.50×10^{-7} to 1.08×10^{-9} mm^3/Nm, respectively, compared with pure oil. Addition of 0.1 wt% of H-BNNPs to PAO6 oil also permitted to reduce both friction coefficient (from 0.1 to 0.07) and wear rate (from 2.5×10^{-7} to 7.2 $\times10^{-8}$ mm^3/Nm).
2. The structural characterization of wear products and *in situ* mechanical testing of BNNPs clearly indicated that the N-BNNPs disintegrated into individual nanosheets which, under applied load, could easily be reoriented parallel to the friction direction, hereby minimizing the resistance to shear. In addition, BN nanosheets formed N-BNNP aggregates uniformly distributed over the area of tribological contact, thus significantly isolating two rubbing surfaces. Such small oiled agglomerates, typically 200–800 nm in size, consist of BN nanosheets which can easily move with respect to each other due to weak Van der Waals forces and thus can be considered as smart flat nanobearings.
3. *In situ* TEM compression tests demonstrated that even under high contact pressure about 1–1.5 GPa the hollow BNNPs mostly restore its initial shape after unloading. This result suggests it is the rolling that was the most likely lubrication mechanism for the H-BNNPs.

Acknowledgments

A.V.B., D.A.S., N.V.S., and D.V.S gratefully acknowledge the financial support from the Russian Scientific Foundation (Agreement No. 14–19-00273-П) in the part of tribological tests. K.L.F. thanks the Ministry of Education and Science of the Russian Federation (Increased Competitiveness Program of NUST “MISiS” No. K2-2016-002) in the part of synthesis of BN nanoparticles. A.M.K. and I.V.S. acknowledges the Ministry of Education and Science of the Russian Federation (Task No. 11.937.2017/ПЧ) in the part of *in situ* mechanical tests.

References

[1] K. Holmberg, P. Andersson, A. Erdemir, Global energy consumption due to friction in passenger cars, Trib. Int 47 (2012) 221–234.
[2] K. Holmberg, R. Siilasto, T. Laitinen, P. Andersson, A. Jäsberg, Global energy consumption due to friction in paper machines, Trib. Intern 62 (2013) 58–77.
[3] K. Holmberg, P. Andersson, N.-O. Nylund, K. Mäkelä, A. Erdemir, Global energy consumption due to friction in trucks and buses, Trib. Int 78 (2014) 94–114.
[4] X. Hou, J. He, L. Yu, Z. Li, Z. Zhang, P. Zhang, Preparation and tribological properties of fluorosilane surface-modified lanthanum trifluoride nanoparticles as additive of fluoro silicone oil, Appl. Surf. Sci. 316 (2014) 515–523.
[5] J. Zhou, Z. Wua, Z. Zhanga, W. Liub, H. Dangа, Study on an antiwear and extreme pressure additive of surface coated LaF_3 nanoparticles in liquid paraffin, Wear 249 (2001) 333–337.
[6] B. Li, X. Wang, W. Liu, Q. Xue, Tribochemistry and antiwear mechanism of organic–inorganic nanoparticles as lubricant additives, Tribol. Lett. 22–1 (2006) 79–84.
[7] B.N. Bakunin, G.N. Kuzmina, M. Kasrai, O.P. Parenago, G.M. Bancroft, Tribological behavior and tribofilm composition in lubricated systems containing surface-capped molybdenum sulfide nanoparticles, Tribol. Lett. 22 (2006) 289–296.
[8] K. Hu, X. Hu, Y. Xu, F. Huang, J. Liu, The effect of morphology on the tribological properties of MoS_2 in liquid paraffin, Tribol. Lett. 40 (2010) 155–165.
[9] L. Rapoport, M. Lvovsky, I. Lapsker, W. Leshchinsky, Y. Volovik, Y. Feldman,

Friction and wear of bronze powder composites including fullerene-like WS_2 nanoparticles, Wear 249 (2001) 149–156.
[10] L.L. Zhang, J.P. Tu, H.M. Wu, Y.Z. Yang, WS_2 nanorods prepared by self-transformation process and their tribological properties as additive in base oil, Mater. Sci. Eng. A 454–455 (2007) 487–491.
[11] X. Kang, B. Wang, L. Zhu, H. Zhu, Synthesis and tribological property study of oleic acid-modified copper sulfide nanoparticles, Wear 265 (2008) 150–155.
[12] Y. Min, M. Akbulut, R.K. Prud'homme, Y. Golan, J. Israelachvili, Frictional properties of surfactant-coated rod-shaped nanoparticles in dry and humid dodecane, J. Phys. Chem. B 112 (2008) 14395–14401.
[13] J.H. Yang, H.X. Yao, Y.Q. Liu, Y.J. Zhang, Synthesis and tribological properties of WSe_2 nanorods, Nanoscale Res Lett. 3 (2008) 481–485.
[14] M.T. Devlin, A.A. Aradi, J.M. Guevremont, T.-C. Jao, V. Abdelsayed, M.S. El-Shall, Friction and film-formation properties of oil-soluble inorganic nanoparticles, SAE Int J. Fuels Lubr. 1 (2009) 1503–1510.
[15] R. Chou, A.H. Battez, J.J. Cabello, J.L. Viesca, A. Osorio, A. Sagastume, Tribological behavior of polyalphaolefin with the addition of nickel nanoparticles, Tribol. Int 43 (2010) 2327–2332.
[16] L. Sun, X. Tao, Y. Zhao, Z. Zhang, Synthesis and tribology properties of stearate-coated Ag nanoparticles, Tribol. Trans. 53 (2010) 174–178.
[17] S. Tarasov, A. Kolubaev, S. Belyaev, M. Lerner, F. Tepper, Study of friction reduction by nanocopper additives to motor oil, Wear 252 (2002) 63–69.
[18] Z. Tang, S. Li, A review of recent developments of friction modifiers for liquid lubricants [2007–present], Curr. Opin. Solid State Mater. Sci. 18 (2014) 119–139.
[19] W. Dai, B. Kheireddin, H. Gao, H. Liang, Roles of nanoparticles in oil lubrication, Tribol. Int 102 (2016) 88–98.
[20] Sun X-f, Xu B-s, Ma S-n, High temperature tribological behaviors of nanodiamond as oil additive, J. Cent. South Univ. Technol. 12 (2005) 181–185.
[21] Y.Y. Wu, W.C. Tsui, T.C. Liu, Experimental analysis of tribological properties of lubricating oils with nanoparticle additives, Wear 262 (2007) 819–825.
[22] L. Rapoport, V. Leshchinsky, M. Lvovsky, O. Nepomnyashchy, Y. Volovik, R. Tenne, Mechanism of friction of fullerenes, Ind. Lubr. Tribol. 54 (2002) 171–176.
[23] M. Kalin, J. Kogovseka, M. Remskar, Mechanisms and improvements in the friction and wear behavior using MoS_2 nanotubes as potential oil additives, Wear 280–281 (2012) 36–45.
[24] Z. Xiaodong, F. Xun, S. Huaqiang, H. Zhengshui, Lubricating properties of cyanex 302-modified MoS_2 microspheres in base oil 500SN, Lubr. Sci. 19 (2007) 71–79.
[25] Z.S. Hu, R. Lai, F. Lou, L.G. Wang, Z.L. Chen, G.X. Chen, J.X. Dong, Preparation and tribological properties of nanometer magnesium borate as lubricating oil additive, Wear 252 (2002) 370–374.
[26] R. Rastogi, M. Yadav, A. Bhattacharya, Application of molybdenum complexes of 1-aryl-2,5-dithiohydrazodicarbonamides as extreme pressure lubricant additives, Wear 252 (2002) 686–692.
[27] G. Liu, X. Li, B. Qin, D. Xing, Y. Guo, R. Fan, Investigation of the mending effect and mechanism of copper nano-particles on a tribologically stressed surface, Tribol. Lett. 17 (2004) 961–966.
[28] P. Rabaso, F. Ville, F. Dassenoy, M. Diaby, P. Afanasiev, J. Cavoret, B. Vacher, T. Le Mogne, Boundary lubrication: influence of the size and structure of inorganic fullerene-like MoS_2 nanoparticles on friction and wear reduction, Wear 320 (2014) 161–178.
[29] I. Lahouij, B. Vacher, J.-M. Martin, F. Dassenoy, IF-MoS_2 based lubricants: influence of size, shape and crystal structure, Wear 296 (2012) 558–567.
[30] R. Rosentsveig, A. Gorodnev, N. Feuerstein, H. Friedman, A. Zak, N. Fleischer, J. Tannous, F. Dassenoy, R. Tenne, Fullerene-like MoS_2 nanoparticles and their tribological behavior, Tribol. Lett. 36 (2009) 175–182.
[31] L. Rapoport, Y. Feldman, M. Homyonfer, H. Cohen, J. Sloan, J. Hutchison, R. Tenne, Inorganic fullerene-like material as additives to lubricants: structure–function relationship, Wear 225 (1999) 975–982.
[32] Y. Xu, E. Hu, K. Hu, Y. Xu, X. Hu, Formation of an adsorption film of MoS_2 nanoparticles and dioctyl sebacate on a steel surface for alleviating friction and wear, Tribol. Int 92 (2015) 172–183.
[33] L. Joly-Pottuz, N. Ohmae, Carbon-based nanolubricants. Nanolubricants, John Willey & Sons, Ltd., 2008, pp. 93–147.
[34] I.V. Sukhorukova, I.Y. Zhitnyak, A.M. Kovalskii, A.T. Matveev, O.I. Lebedev, X. Li, N.A. Gloushankova, D. Golberg, D.V. Shtansky, BN nanoparticles with petal-like surface as anticancer drug delivery system, ACS Appl. Mater. Interfaces 7 (2015) 17217–17225.
[35] A.M. Kovalskii, A.T. Matveev, O.I. Lebedev, I.V. Sukhorukova, K.L. Firestein, A.E. Steinman, D.V. Shtansky, D. Golberg, Growth of spherical boron oxynitride nanoparticles with smooth and petalled surfaces during chemical vapor deposition process, CrystEngComm 18 (2016) 6689–6699.
[36] D.-H. Cho, J.-S. Kim, S.-H. Kwon, C. Lee, Y.-Z. Lee, Evaluation of hexagonal boron nitride nano-sheets as a lubricant additive in water, Wear 302 (2013) 981–986.
[37] O.N. Çelik, N. Ay, Y. Göncü, Effect of nano hexagonal boron nitride lubricant additives on the friction and wear properties of AISI 4140 steel, Part Sci. Technol. Int J. 3 (2013) 501–506.
[38] Q. Zeng, F. Yu, G. Dong, Superlubricity behaviors of Si_3N_4/DLC films under PAO oil with nano boron nitride additive lubrication, Surf. Interface Anal. 45 (2013) 1283–1290.
[39] J. Taha-Tijerina, T.N. Narayanan, G. Gao, M. Rohde, D.A. Tsentalovich, M. Pasquali, P.M. Ajayan, Electrically insulating thermal nano-oils using 2D fillers, Am. Chem. Soc. 6 (2012) 1214–1220.
[40] Q. Wan, Y. Jin, P. Sun, Y. Ding, Tribological behaviour of a lubricant oil containing boron nitride nanoparticles, Procedia Eng. 102 (2015) 1038–1045.
[41] S. Kumari, O.P. Sharma, R. Gusain, H.P. Mungse, A. Kukrety, N. Kumar, H. Sugimura, O.P. Khatri, Alkyl-hain-grafted hexagonal boron nitride nanoplatelets as oil-dispersible additive for friction and wear reductions, ACS Appl. Mater. Interfaces 7 (2015) 3708–3716.
[42] Y. Kimura, T. Wakabayashi, K. Okada, T. Wada, H. Nishikawa, Boron nitride as a lubricant additive, Wear 232 (1999) 199–206.
[43] D.-H. Cho, J.-S. Kim, S.-H. Kwon, C. Lee, Y.-Z. Lee, Evaluation of hexagonal boron nitride nano-sheets as a lubricant additive in water, Wear 302 (2013) 981–986.
[44] Abdullah MIHC, Abdollah MFB, H. Amiruddin, T. Tamaldin, Nuri RMN, Optimization of tribological performance of hBN/Al_2O_3 nanoparticles as engine oil additives, Procedia Eng. 68 (2013) 313–319.
[45] D.V. Shtansky, O. Tsuda, Y. Ikuhara, T. Yoshida, Crystallography and structural evolution of cubic boron nitride films during bias sputter deposition, Acta Mater. 48 (2000) 3745–3759.
[46] J. Padgurskas, R. Rukuiza, I. Prosyčevas, R. Kreivaitis, Tribological properties of lubricant additives of Fe, Cu and Co nanoparticles, Tribol. Int 60 (2013) 224–232.
[47] L. Chen, D. Zhu, Preparation and tribological properties of unmodified and oleic acid-modified CuS nanorods as lubricating oil additives, Ceram. Int 43 (2017) 4246–4251.
[48] M. Kalin, J. Kogovšeka, M. Remškar, Mechanisms and improvements in the friction and wear behavior using MoS_2 nanotubes as potential oil additives, Wear 280–281 (2012) 36–45.
[49] A. Hernandez Battez, J.E. Fernandez Rico, A. Navas Arias, J.L. Viesca Rodriguez, R. Chou Rodriguez, J.M. Diaz Fernandez, The tribological behaviour of ZnO nanoparticles as an additive to PAO6, Wear 261 (2006) 256–263.
[50] O. Goldbart, A. Sedova, L. Yadgarov, R. Rosentsveig, D. Shumalinsky, L. Lobik, H.D. Wagner, R. Tenne, Lubricating medical devices with fullerene-like nanoparticles, Tribol. Lett. 55 (2014) 103–109.